



## Report on the optical and electric properties of the nitrate compound crystals

メタデータ	言語: eng 出版者: 室蘭工業大学 公開日: 2014-03-04 キーワード (Ja): キーワード (En): 作成者: 川島, 利器, 福田, 明治, 勝木, 喜一郎, 鈴木, 和郎 メールアドレス: 所属:
URL	<a href="http://hdl.handle.net/10258/751">http://hdl.handle.net/10258/751</a>

# Report on the optical and electric properties of the nitrate compound crystals

川 島 利 器 · 福 田 明 治 · 勝 木 喜 一 郎 · 鈴 木 和 郎

Riki Kawashima, Akeharu Fukuda, Kichiro Katsuki and Kazuo Suzuki

## Abstract

The crystals of nitrates show various phase transitions. The crystal structure changes near the transition temperature  $T_{tr}$ . The characteristic phenomena, associated with the physical properties have been observed near the phase transition points. The optical and electric properties have been reported in the temperature region of the alkali and the rare earth nitrate crystals.

## 1. Introduction

The variation in the physical properties of the crystals are observed near the phase transition points<sup>(1)</sup>. The nitrates are among the few readily soluble and easily prepared inorganic compounds. The crystal of the nitrate is a dielectric one, which shows a various phase transition with the change in the crystal structure. The authors have investigated the optical<sup>(2)</sup> and electric properties<sup>(3)</sup> of the nitrate crystals near their phase transition points. In this paper, we report on the optical and electric properties of the alkali and rare earth nitrate crystals in our investigation, which is proceeding in the present stage.

## 2. Experimental Procedures

### 2.1 Crystal Growth

Single crystals used in these experiments were prepared as follows by using the solution method. An aqueous solution of nitrate compound was prepared from the nitrate powder. To remove dust and impurities insoluble in water, the solution of nitrate was filtered with micron filter of  $0.2 \mu\text{m}$  pore size. The single crystals were grown from the aqueous solution by slow evaporation at room temperature.

### 2.2 Optical Measurement

The optical measurement was made in the following way<sup>(2)</sup>. A ploy-chromatic light source

(deuterium lamp) is chopped at 175 Hz. The incident light beam was made nearly perpendicular to the prepared plane of the single crystal. The fluctuation of the light intensity was within 1%. A Nikon P-250 monochromator was used, whose diffraction grating (1200 lines per cm) gives a resolution of 1 Å by using the following experimental conditions: height of the slits 4 mm: width of the slits, 0.01 mm: scanning speed, 450~150 Å/min for the observation of full spectrum range. The beam diffracted by the monochromator was received by a photomultiplier R-189 (HTV), connected with a Nikon SP104 electrometer. Temperature dependence of the absorption spectrum was measured by using the furnace. The temperature of sample was detected by a alumel-chromel thermocouple, the signal of which was also utilized for controlling the furnace temperature. Temperature of the sample was less than 0.01°C. Temperature of the sample was changed from room temperature to 350°C.

### 2.3 Electric Measurement

We have measured the frequency dependence of AC impedance of the crystal by using an auto-phase lock in amplifier (NF Electronic Instrum., LI-574A with pre-amp. P-51A) and wide band oscillator (NF Electronic Instrum., E-1205)<sup>(3)</sup>. Specimens were prepared by cutting the crystal parallel to the observed plane: the typical dimension of sample is  $0.047 \pm 0.005$  cm in thickness and  $0.096 \pm 0.005$  cm<sup>2</sup> in area. The silver electrodes were pasted on the surfaces. The measurements were performed in the course of heating and cooling. The specimen was placed in a furnace controlled to  $\pm 0.1^\circ\text{C}$ .

## 3. Results

### 3.1 Optical absorption spectrum

The single crystal of robidium nitrate, as one of the alkali nitrate crystals, undergoes three phase transitions<sup>(4)</sup>. The orthorhombic phase (IV) changes to a cubic (SsCl-type) phase (III) at  $\sim 164^\circ\text{C}$ , then to rhombohedral type phase (II) at  $\sim 219^\circ\text{C}$  and finally to NaCl type cubic phase (I) at  $\sim 285^\circ\text{C}$ . The successive phase transitions are related with orientational disorder of the  $\text{NO}_3^-$  ions.

Figure 1, as already given in Ref.(2), shows the absorption spectra in the photon energy region from 3.10 eV to 5.0 eV at temperatures in the phases IV, III and II of  $\text{PbNO}_3$  crystal. The two absorption bands, corresponding to the  $n_2 \rightarrow \pi^*$  and  $\pi_2 \rightarrow \pi^*$  band<sup>(5)</sup>, are contained in the region from 3.10 eV to 5.0 eV for the alkali nitrate crystal. The absorption band from 3.50 to 4.50 eV has been assigned to the  $n_2 \rightarrow \pi^*$  forbidden intramolecular electronic transition of the  $\text{NO}_3^-$  ions in

the  $\text{RbNO}_3$  crystal. The stronger absorption band above 4.50 eV has been assigned to the  $\pi_2 \rightarrow \pi^*$  allowed electronic transition of the ion.

### 3.2 Electric Conductivity

Figure 2 shows temperature dependence of the real part  $\sigma'$  and the imaginary part  $\sigma''$  of the complex conductivity derived from the measurements of the AC impedance at 1 kHz along the  $c$ -axis of the  $\text{RbNO}_3$  crystal in the temperature region from temperature to  $236^\circ\text{C}$ , ranged over the IV $\rightarrow$ III and III $\rightarrow$ II successive phase transition points. This result has already been given in Ref.(3). The hystereses of  $\sigma'$  and  $\sigma''$  near the IV $\rightarrow$ III and III $\rightarrow$ II phase transition points are found in Fig. 2.

Frequency dependence of  $\sigma'$  and  $\sigma''$  (the real part  $\sigma'$  corresponding to conductivity and the imaginary part  $\sigma''$  to dielectric constant) in the complex conductivity is measured over the range

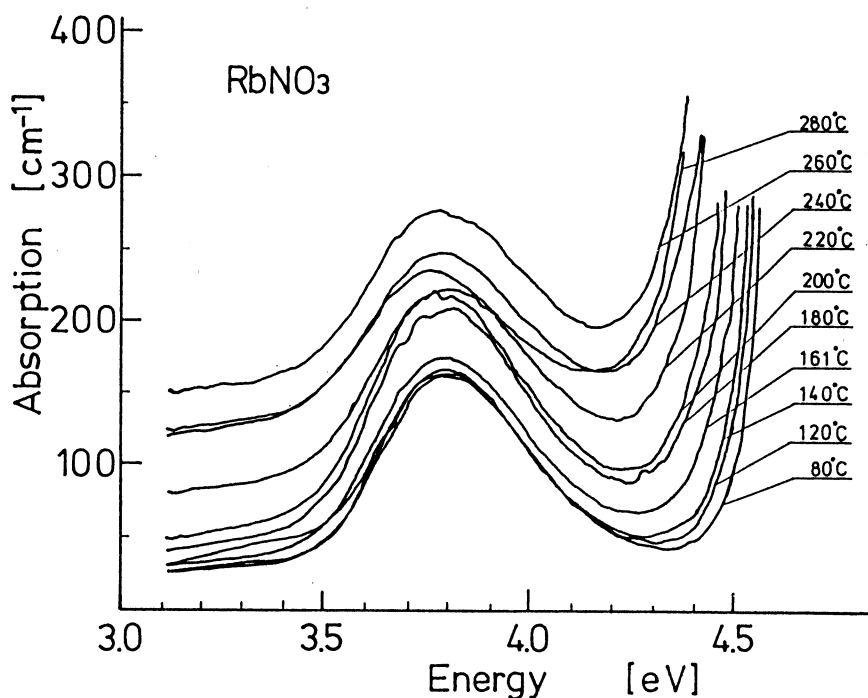


Fig. 1 Temperature dependence of the absorption spectrum  $\alpha(E, T)$  at several temperatures ranged from room temperature to  $280^\circ\text{C}$ .

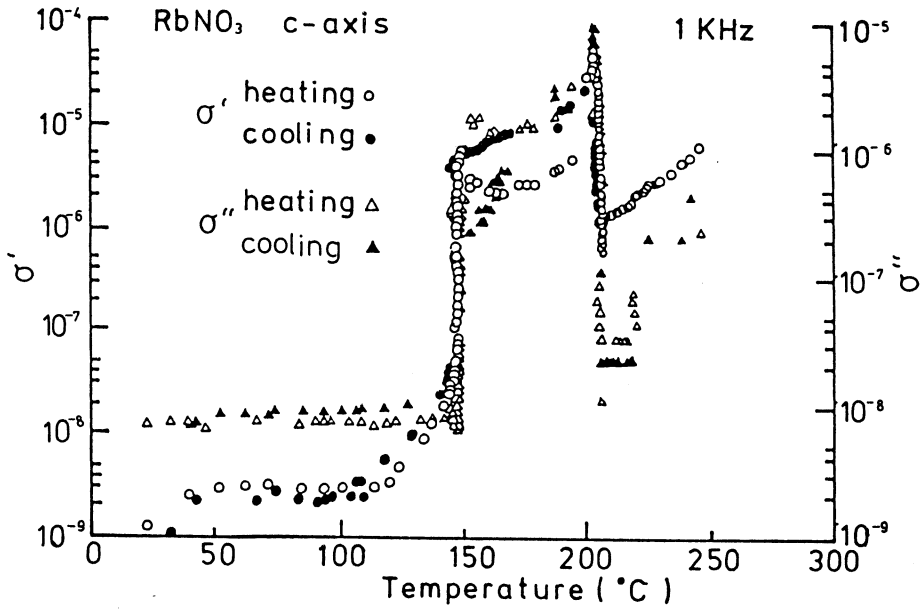


Fig. 2 Temperature dependence of real  $\sigma'$  and imaginary  $\sigma''$  in the complex conductivity  $\sigma^*$  measured by the AC impedance method along the c-axis of  $\text{RbNO}_3$  crystal at 1 KHz in the course of heating and cooling after Ref.(3).

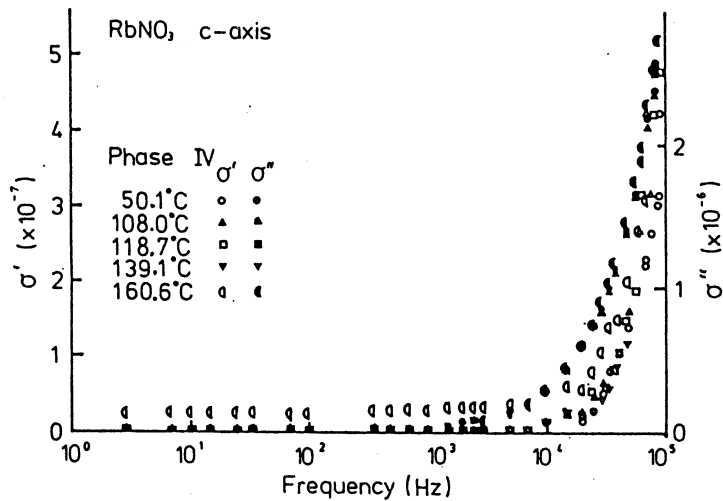


Fig. 3 Frequency variation of the real  $\sigma'$  and imaginary  $\sigma''$  in the complex conductivity  $\sigma^*$  measured by the AC impedance method along the c-axis of  $\text{RbNO}_3$  crystal at temperatures in the phase IV after Ref.(3).

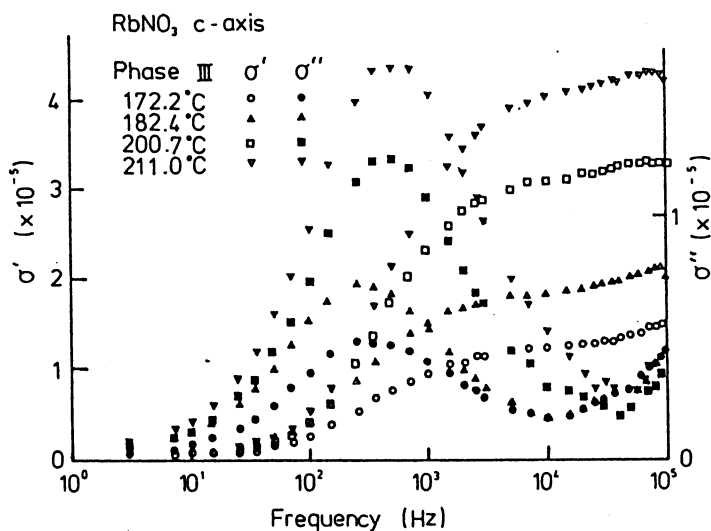


Fig. 4 Frequency variation of  $\sigma'$  and  $\sigma''$  in the complex conductivity  $\sigma^*$  measured by the AC impedance method along the c-axis of RbNO<sub>3</sub> crystal at temperatures in the phase III after Ref.(3).

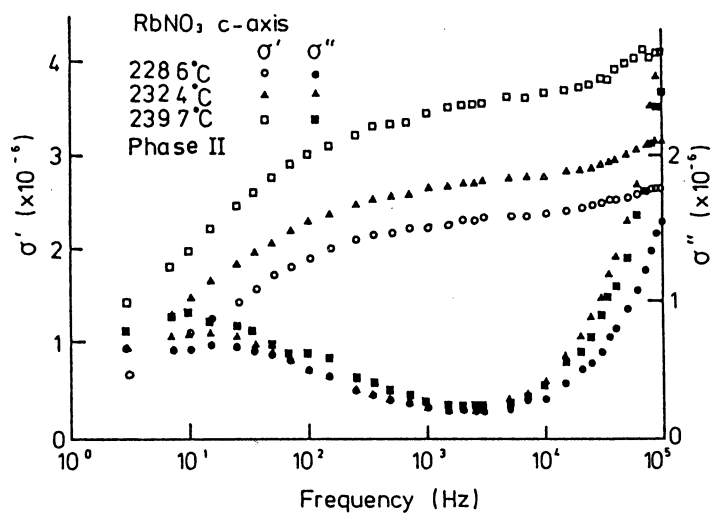


Fig. 5 Frequency variation of  $\sigma'$  and  $\sigma''$  in the complex conductivity  $\sigma^*$  measured by the AC impedance method along the c-axis of RbNO<sub>3</sub> crystal at temperatures in the phase II after Ref.(3).

from 3 Hz to 100 kHz at several temperatures, respectively, in the phases IV, III and II. Figures 3, 4 and 5 show the frequency dependence of conductivities  $\sigma'$  and  $\sigma''$  in the phases IV, III and II, respectively, of the  $\text{RbNO}_3$ . These results have already been reported in Ref.(3).

## 4. Discussion

### 4.1 Optical properties near the phase transitions of alkali nitrates

The author and his collaborators<sup>(2)</sup> have given the experimental results and the analyses on the temperature dependence of the absorption spectra, in the alkali nitrate crystals, ascribed to both the  $n_2 \rightarrow \pi^*$  and  $\pi^*$  bands by using the profile model given in Ref.(6) for studying the absorption spectra in the  $\text{RbNO}_3$  melt. In the model, the spectrum consisted of the sum of a Gaussian function, identified with the  $n_2 \rightarrow \pi^*$  band, and an exponential function, identified with the edge of the  $\pi_2 \rightarrow \pi^*$  band,

$$\alpha = \alpha_{Max} \exp \left\{ -\frac{(\ln 2)(E - E_{Max})^2}{(\Delta E)^2} \right\} + \alpha_o \exp \left\{ \sigma(T)(E - E_o)/K_B T \right\} \quad (1)$$

For the Gaussian assigned to the  $n_2 \rightarrow \pi^*$  band,  $\alpha_{Max}$  and  $E_{Max}$  of the first term in the above equation are the coordinates of the maximum of the  $n_2 \rightarrow \pi^*$  band. On the other hand, as the second term in the right side of Eq.(1), the edge of the  $\pi_2 \rightarrow \pi^*$  band exhibits exponential shape obeying the Urbach rule. Where  $\alpha_o$  and  $E_o$  are constants determining the coordinates of the intersection point of extrapolated linear sections of absorption curves  $\alpha = f(\hbar\omega, T)$ , and where a parameter  $\alpha(T)$  is called as the steepness one<sup>(7)</sup>.

The digitized data obtained by the A/D converter of the optical measurements were fitted to the model given in Eq.(1) by using a micro-computer PC9801E(NEC). By the digital computer procedures for the profile analysis on the basis of the model given in Eq.(1), the  $\pi_2 \rightarrow \pi^*$  band was separated from the overlapping absorption edge. Figure 6 shows the spectra obtained by the analyses, at temperatures between 80°C and 280°C, in the vicinity of the tails of the  $\pi_2 \rightarrow \pi^*$  band spectra.

Figure 7 shows these data plotted as  $\log \alpha$  vs.  $E$  at several temperatures in the phase IV, III and II for the tail of the separated  $\pi_2 \rightarrow \pi^*$  band spectra. From the numerical analyses on the tails of the separated  $\pi_2 \rightarrow \pi^*$  band spectra, as given in Ref.(11), the values of  $E_o$  and  $\alpha_o$  have been determined:  $E_o = 4.80 \pm 0.10$  eV and  $\alpha_o = 3000 \pm 10 \text{ cm}^{-3}$  for the IV phase:  $E_o = 4.75 \pm 0.09$  eV and  $\alpha_o = 2000 \pm 10 \text{ cm}^{-1}$  for the III phase:  $E_o = 4.60 \pm 0.10$  eV and  $\alpha_o = 1000 \pm 10 \text{ cm}^{-1}$  for the II phase.

Figure 8, after Ref(1), shows the temperature dependence of the slope parameter  $\sigma(T)$  derived from the results analyzed from the data on the base of the profile model. The anomalies of  $\sigma(T)$  are found at the phase transition points. The behaviors of the absorption edge, as given in Figs. 7 and 8, and as described by the values of  $E_0$  and  $\alpha_0$  is not classified into the limiting cases of the Urbach edge<sup>(8)</sup>, slope parameter  $\sigma(T)$ , and the absorption edge shift, as function of temperature: anomaly of  $\sigma(T)$  only, of  $E_0$  only, of  $\alpha_0$  only and no anomaly at the phase transition point.

The shift of  $E_0$  is in direct relation to the change in the width between the energy levels in the intramolecular state of  $\text{NO}_3^-$ , corresponding to the forbidden band width in the Urbach rule discussed in the semiconductor or ionic crystal<sup>(7)</sup>. On the other hand, the parameter  $\sigma(T)$  is given by,

$$\sigma(T) = \sigma_0 \frac{2k_B T}{\hbar \omega} \tanh(\hbar \omega / 2k_B T), \quad (2)$$

where  $\hbar \omega$  is the energy of effective phonon, most strongly coupled with the electronic processes or excitons.  $\alpha_0$  is a constant represented the strength of the electron-phonon interaction or exciton-phonon interaction. At high temperatures ( $k_B T \gg \hbar \omega$ ),

$$\sigma(T) \sim \sigma_0 \quad (3)$$

The variation in  $\sigma(T)$  may be due to either a change in the electron-phonon or exciton-phonon in-

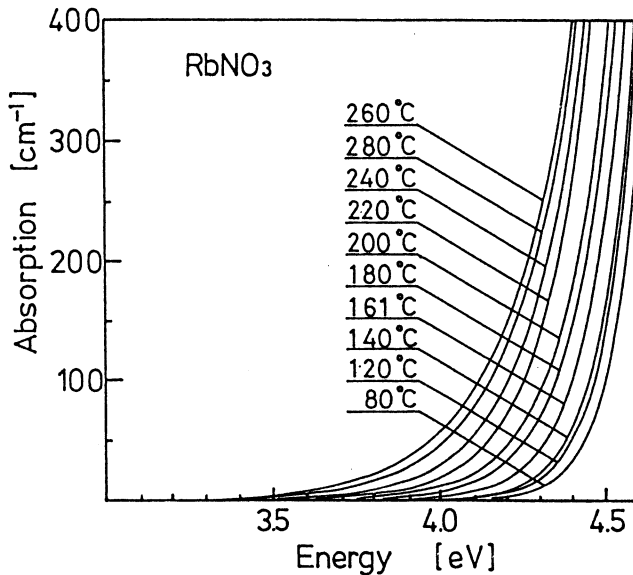


Fig. 6 Temperature dependence of the  $\pi_2 \rightarrow \pi^*$  band spectra separated from the observed spectra at temperatures ranged from 80°C to 280°C.

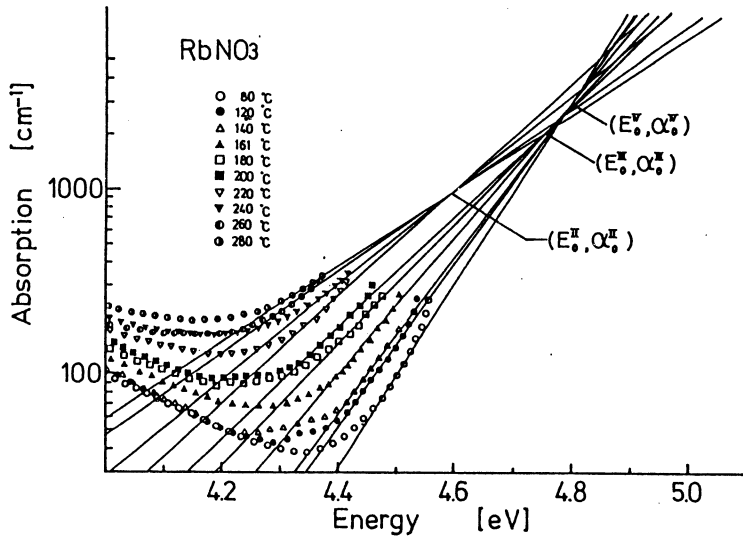


Fig. 7 The linear relationship of  $\log \alpha$  (cm<sup>-1</sup>) vs. photon energy  $E$  (eV) of the absorption edge at several temperatures ranged from 80°C to 280°C.

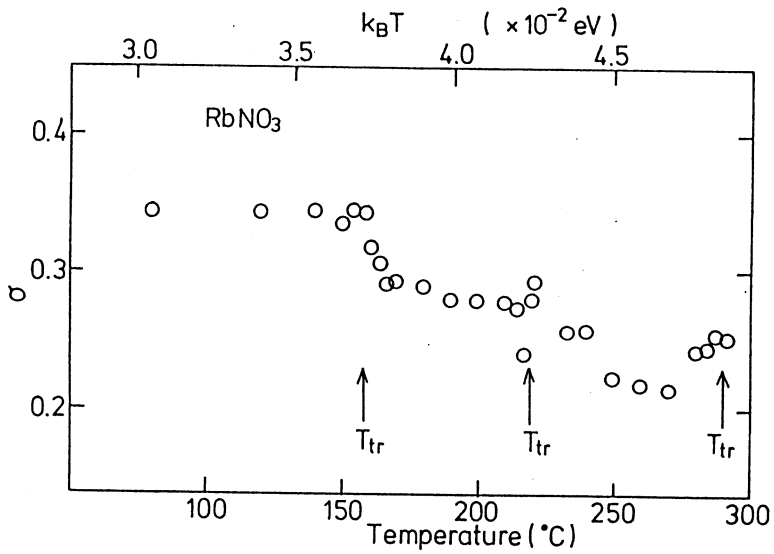


Fig. 8 The steepness parameter  $\sigma$  (T) derived as a function of thermal energy  $k_B T$  (eV) and Temperature (°C) for the RbNO<sub>3</sub> crystal after Ref.(2).

teraction strength through  $\alpha_0$  or to a possible change of the phonon, the instability of phonon mode, coupled to electron or exciton near the phase transitions.

Overall values of  $\sigma$  (T) in both the phases IV, III and II of  $\text{RbNO}_3$  crystal are less than 1.0. Line shapes of the absorption-band have been discussed in simple ionic crystals<sup>(7)</sup>. The type of the electronic process, associated with the optical absorption, has been classified by a criterion attributed to the  $\sigma$  values. Though the  $\text{RbNO}_3$  crystal has more complicated crystal structures, it may be inferred from  $\sigma < 1.0$  that the electronic process in three phases of the crystal is of localized type as suggested in the case of other alkali nitrate crystals<sup>(2)</sup>;  $\text{LiNO}_3$ ,  $\text{NaNO}_3$ ,  $\text{KNO}_3$ ,  $\text{CsNO}_3$ . The results could suggest that the intramolecular electronic state of the  $\text{NO}_3^-$  ion in the alkali nitrate crystal is of localized type.

Line shapes of the absorption spectra for the  $n_2 \rightarrow \pi^*$  band have been separated from the measured overlapping absorption ones at each temperatures, in the  $\text{RbNO}_3$  crystal. The  $n_2 \rightarrow \pi^*$  absorption is represented in the form,

$$\alpha' = \alpha_{\text{Max}} \exp \left\{ -(1/2)(E - E_{\text{Max}})^2 / (\Delta E)^2 \right\} . \quad (4)$$

The value of  $E_{\text{Max}}$  is that of the energy of the maximum of the  $n_2 \rightarrow \pi^*$  band. In the temperature range over the phases IV and III, the value of  $E_{\text{Max}}$  is independent of temperature, as defined by 3.79 eV, within experimental accuracy. On the other hand, the value of  $E_{\text{Max}}$  in the phase II is determined by 3.78 eV. This result is consistent with that of the spectra obtained in the molten  $\text{RbNO}_3$ . The  $n_2 \rightarrow \pi^*$  band itself does not shift in the  $\text{RbNO}_3$  crystal, as this behavior of  $E_{\text{Max}}$  is similar to that obtained in the  $\text{CsNO}_3$  crystal, but different to that observed in the  $\text{NaNO}_3$  crystal.

The temperature dependence of the half-value width  $\Delta E(T)$  for the  $n_2 \rightarrow \pi^*$  band is plotted in Figure 9, referred to Ref.(2), for the  $\text{RbNO}_3$  crystal. The value of  $\Delta E(T)$  increase by increasing temperature, but show stepwise variation at the successive phase transition points. Figure 10 shows these data plotted as  $\Delta E(T)$  vs. T in both the phase II and I of  $\text{NaNO}_3$  crystal. As seen from Fig. 10, the values of  $\Delta E(T)$  changes near the  $\lambda$  transition point of  $\text{NaNO}_3$ . The phase transitions of alkali nitrate crystals are attributed to the orientational disorder-ordered state of the  $\text{NO}_3^-$  ions. The  $\text{NO}_3^-$  ions show free rotation along the c-axis in the phase I of  $\text{NaNO}_3$ . The increase of  $\Delta E(T)$  with increasing temperature in the phase I could be related to the dynamical state of  $\text{NO}_3^-$ .

The line width of the absorption band has been discussed in the relation with thermal broadening due to the coupling of the electronic process to lattice vibrations<sup>(9)</sup> and with the external and internal fluctuations of vibronic states corresponded with inhomogeneous broadening<sup>(10)</sup>. The  $n_2 \rightarrow \pi^*$  absorption band has been assigned to the vibronic intramolecular electronic transition in the

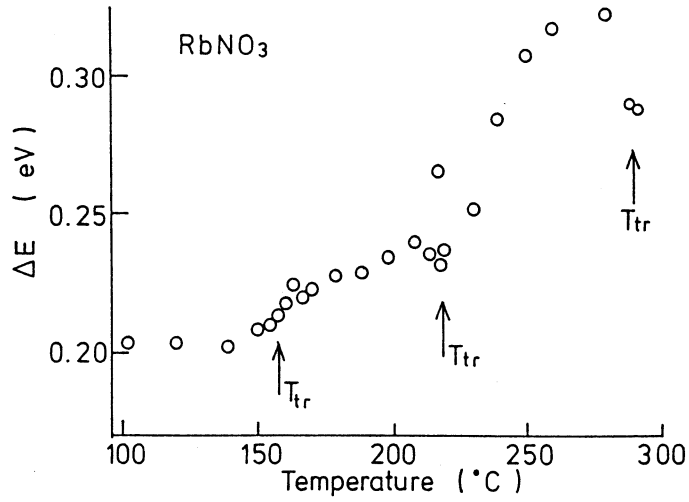


Fig. 9 Temperature dependence of the half-valued width  $\Delta E$  of the  $n_2 \rightarrow \pi^*$  absorption band for the RbNO<sub>3</sub> crystal after Ref.(2).

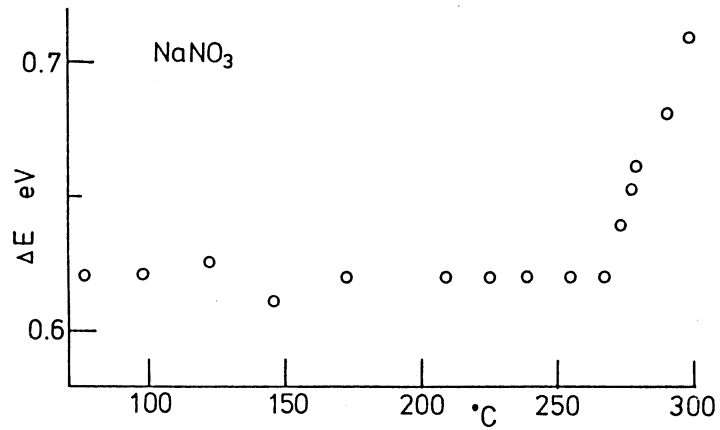


Fig. 10 Temperature dependence of the half-valued width  $\Delta E$  of the  $n_2 \rightarrow \pi^*$  absorption band for the NaNO<sub>3</sub> crystal.

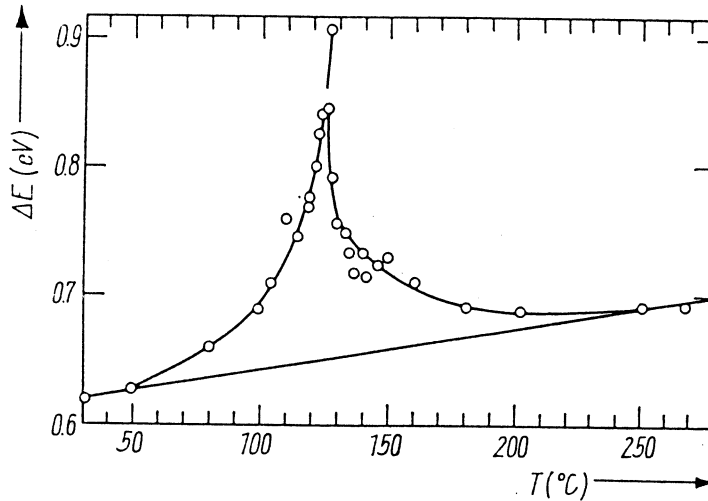


Fig. 11 Temperature dependence of the half-valued width  $\Delta E$  of the  $n_2 \rightarrow \pi^*$  absorption band for the  $\text{KNO}_3$  crystal after Ref.(2).

$\text{NO}_3^-$  ions. In the case, the behavior of  $\Delta E(T)$  could depend on the variation in the thermal fluctuation in the molecular structure and dynamical state of  $\text{NO}_3^-$  ions themselves or distribution of the different environment around the ions.

Various types of the anomalous behaviors (a maximum peak, a minimum dip or stepwise change) in the thermodynamical coefficients<sup>(11)</sup> (dielectric constant, conductivity, heat capacity, elastic coefficient, ultrasonic attenuation etc.) have been observed near the phase transition point. The variation, in the variables to describe the physical property of the crystal<sup>(33)</sup>, could be dependent on the type of the coupling of the variable with the order parameter of the phase transition. The properties of the coupling could be determined by the symmetry of crystal in the phenomenological theory on the structural phase transition. In the ultrasonic studies<sup>(12)</sup>, for example, as the elastic strain induced by the ultrasonic wave couples linearly with the order parameter, the elastic constant, derived from the ultrasonic velocity, do a maximum peak at the phase transition point. But in the case of the nonlinear coupling, the coefficient shows a stepwise variation at the temperature.

The line width  $\Delta E(T)$  shows a sharp peak near the  $\text{II} \rightarrow \text{I}$  phase transition point of the  $\text{KNO}_3$  crystal in Figure 11, as reported in Ref.(2), but do not in the vicinity of the successive phase transition points of  $\text{RbNO}_3$  as seen in Fig. 9. The facts would suggest the linear coupling between the intramolecular electronic process and the order parameter in the limited case of the alkali nitrate crystal such as the  $\text{KNO}_3$  crystal. In the case of the  $\text{RbNO}_3$  crystal, however, the order parameter could not couple linearly with the electronic property in the  $\text{NO}_3^-$  ion.

#### 4.2 Electric properties near the phase transitions of alkali nitrate crystals

The conductivity of the alkali nitrate crystal is attributed to the cation Frenkel defects<sup>(13)</sup>. The temperature dependence of the transport property near the successive phase transition points of the  $\text{RbNO}_3$  crystal has been qualitatively interpreted by the change of the crystal structure<sup>(14)</sup>.

The large increase of the electric conduction at the IV $\rightarrow$ III phase transition point is ascribed to the fact that the shortest distance (3.63Å) of  $\text{NO}_3^-$  from  $\text{Rb}^+$  in the phase III is greater than the sum (3.42Å) of the radii of the  $\text{NO}_3^-$  groups (1.94 Å) and  $\text{Rb}^+$  ion (1.48 Å). In the cube of phase III, the  $\text{NO}_3^-$  group lies on the body diagonal slightly shifted from the center. In the rhombohedron of the phase II, also, the  $\text{NO}_3^-$  group remains in an off-center position to the same relative extent as in the phase III. The distance between the  $\text{NO}_3^-$  group and the three nearest  $\text{Rb}^+$ , surrounding the body diagonal, becomes equal to 3.32 Å in the rhombohedron of phase II. This distance is smaller than the sum of the radii of the  $\text{NO}_3^-$  group and the  $\text{Rb}^+$  ion. The  $\text{NO}_3^-$  ions are locked in an off-center position on the body diagonal so that its movement on it is hampered, leading to the decrease of the conductivity at the III $\rightarrow$ II phase transition point.

These electric properties in the phases IV, III and II of the  $\text{RbNO}_3$  crystal could be described by complex plane of the complex conductivity (known as the Grant Plots<sup>(15)</sup>). The present discussion on the properties have been referred to Ref.(3). Figure 12 shows the conductivity of the phase IV

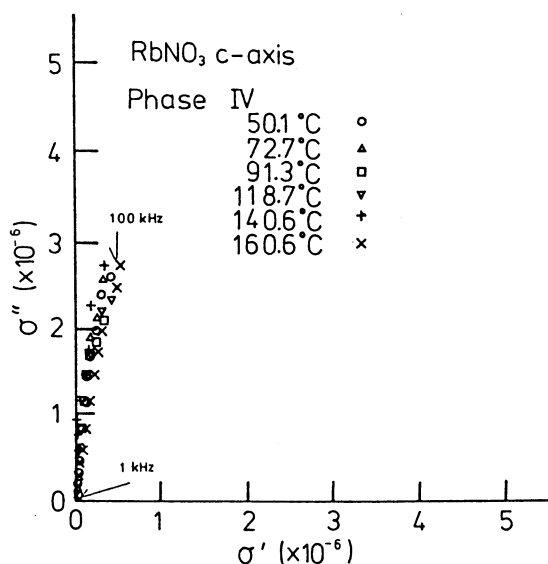


Fig. 12 Representation of the conductivity along the c-axis in the complex plane ( $\sigma''$  vs  $\sigma'$ ) at temperatures in the IV phase of the  $\text{RbNO}_3$  crystal after Ref.(3).

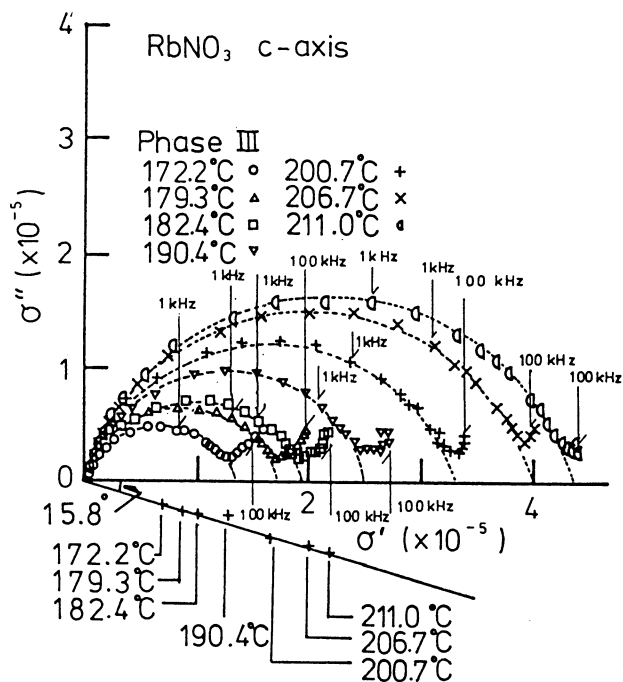


Fig. 13 Representation of the conductivity along the c-axis in the complex plane ( $\sigma''$  vs  $\sigma'$ ) at temperatures in the III phase of the RbNO<sub>3</sub> crystal after Ref.(3).

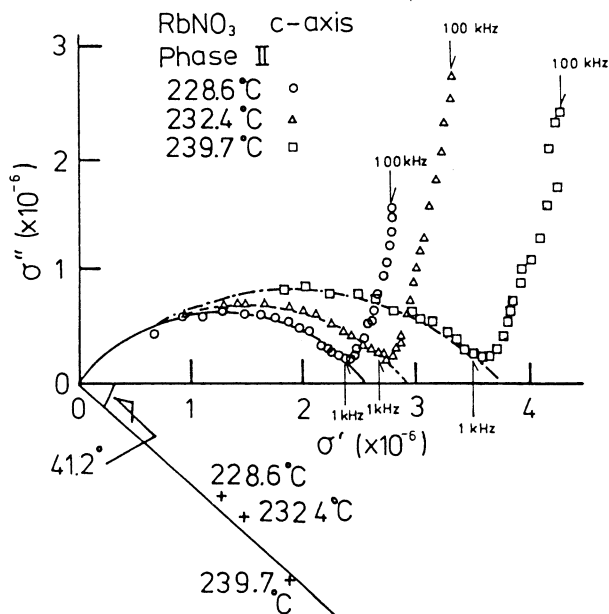


Fig. 14 The complex conductivity ( $\sigma''$  vs  $\sigma'$ ) along the c-axis at temperatures in the II phase of the RbNO<sub>3</sub> crystal after Ref.(3).

plotted in the complex plane. The values of  $\sigma'$  at  $\sigma''=0$  increase with approaching the IV $\rightarrow$ III phase transition point. The frequency dispersion of the normal dielectric crystal has been usually observed in the frequency region above  $\sim 1$  MHz. The observed dispersion in the phase IV near the IV $\rightarrow$ III phase transition point corresponds to the tail in the lower frequency side of the Cole-Cole semicircle.

Figure 13 shows the frequency dependence of the complex conductivity in the complex plane,  $\sigma''$  vs  $\sigma'$ , at temperatures of the phase III. The complex conductivity in the phase III can be represented by semi-circles with centers below the real axis  $\sigma'$ . The centers lie on the line making an angle  $\alpha = 15.8^\circ$  with the real axis. This dispersion in the phase III is similar to that in the ferroelectric materials<sup>(16)</sup> with the distributed relaxation time. This result is different from that obtained by measuring the AC electric conductivity along the *a*-axis of the crystal.

The frequency variation of the complex conductivity in the complex plane at several temperatures of the phase II is given in Figure 14. In this phase, the spectra in the complex conductivity also fit the semi-circles. The centers of the semicircles at the temperatures lie below the real axis with the deviated angle  $\alpha = 41.2^\circ$ .

These diagrams given in Figs. 13 and 14 show that in the temperature region of the phases III and II, the frequency dispersion of the complex conductivity  $\sigma^*(T, \omega)$  can be given by

$$\{ \sigma^*(T, \omega) - \sigma(T, \infty) \} / \{ \sigma(T, 0) - \sigma(T, \infty) \} \quad (5)$$

in which the adjustable parameter  $\beta$  indicates the degree of distribution of the relaxation time. The parameter  $\beta$  is given by the angle  $\alpha$  of the Cole-Cole diagram through the relation  $\beta = 1 - 2\alpha/\pi$  ( $\alpha$  in the radian unit);  $\beta = 0.53$  in the phase II and  $\beta = 0.82$  in the phase III. This value of  $\beta$  derived in the phase II of the RbNO<sub>3</sub> crystal is nearly equal to that,  $0.52 \sim 0.57$ , given in the dielectric measurement on the phase I of the KNO<sub>3</sub> crystal<sup>(17)</sup>. The crystal structure, R3m, in the phase II of RbNO<sub>3</sub> is the same<sup>(18)</sup> as that in the phase I of KNO<sub>3</sub>. The fact suggests the similarity between the dielectric relaxation processes of these crystals. However, the dielectric spectrum in the phase I of KNO<sub>3</sub> was observed in the range from 15 GHz to 22.3 GHz.

### 4.3 Phase transition of Rare earth compound crystals

Recently, investigation of rare earth compounds has received considerable attention to study the physical properties associated with rare earths spectroscopy<sup>(19)</sup>, valence instability<sup>(21)</sup>, high temperature superconductivity (rare earth oxides)<sup>(22)</sup> and ferroelectricity and ferroelasticity (Gd<sub>2</sub>(MoO<sub>4</sub>)<sub>3</sub> family)<sup>(11)</sup>.

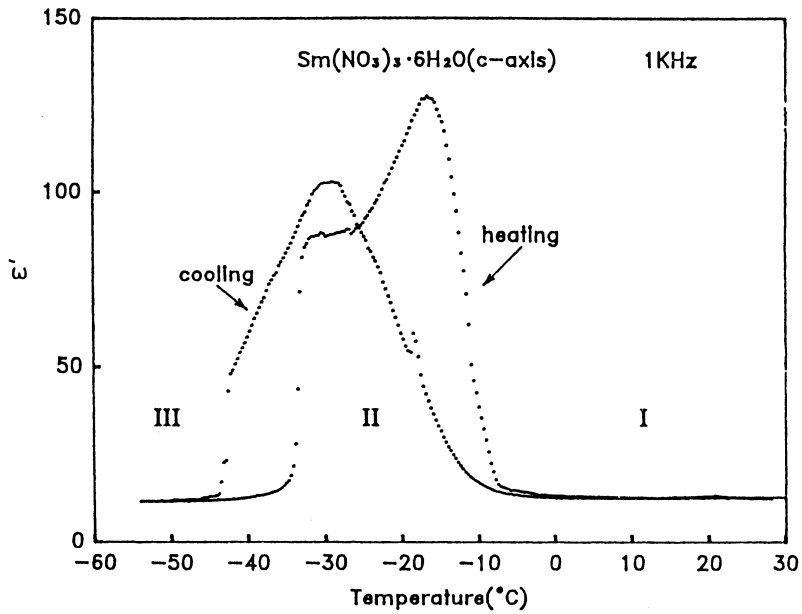


Fig. 15 The real part  $\epsilon'$  of complex dielectric constant  $\epsilon^*$  along the c-axis of samarium nitrate crystal at temperatures in the range between room temperature and  $-55.0^\circ\text{C}$  in both the cooling and warming processes after Ref.(3).

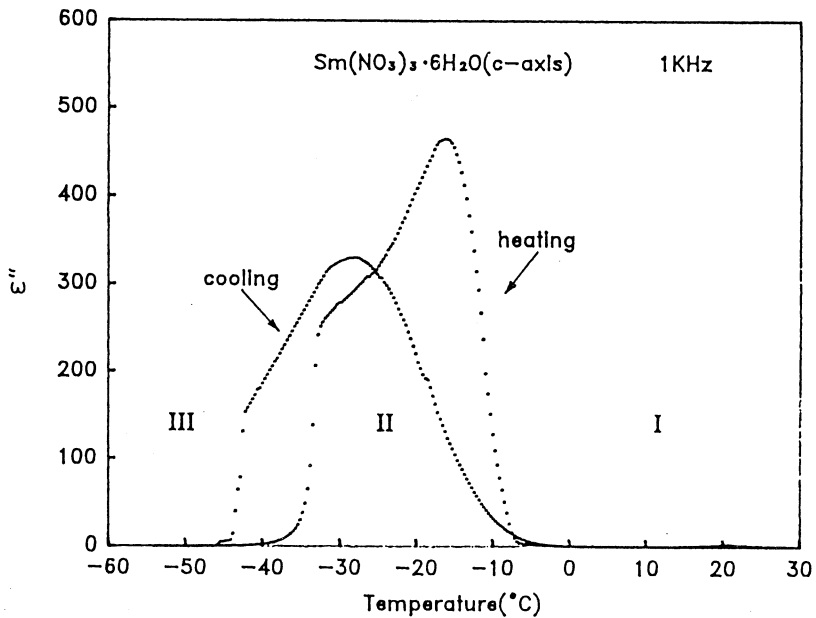


Fig. 16 The imaginary part  $\epsilon''$  of complex dielectric constant  $\epsilon^*$  along the c-axis of samarium nitrate crystal at temperatures in the range between room temperature and  $-55.0^\circ\text{C}$  in both the cooling and warming processes after Ref.(3).

In the material system, a rare earth ion plays an important role for the characteristic properties. The nitrates are among the few soluble and easily prepared inorganic compounds of the rare earths. It is possible to find unknown physical phenomena in the crystals of rare earth nitrates. In the present section, the experimental results on the samarium nitrate crystal are given by the electric measurement with the automatic system in order to study the phase transition of samarium nitrate crystal in detailed.

The temperature dependence of the real  $\epsilon''$  and the imaginary part  $\epsilon''$  at 1KHz are given in Figures 15 and 16 of both heating and cooling run in the range from room temperature to  $-55^\circ\text{C}$ . From the results, two singularities with thermal hystereses are found in the temperature variation of dielectric constants.

The anomalous temperature dependence of the dielectric constants between  $\sim -45^\circ\text{C}$  and  $\sim 0^\circ\text{C}$  should be related to polymorphic transitions with the change of the crystal structure in the samarium nitrate crystal. The crystal symmetry of samarium nitrate crystal,  $\text{Sm}(\text{NO}_3)_3 \cdot 6\text{H}_2\text{O}$ , is triclinic, the space group  $\text{P}\bar{1}$  with lattice parameters of  $a=9.20$  A,  $b=11.7$  A,  $c=6.78$  A,  $\alpha=91$ ,  $\beta=112^\circ$  and  $\gamma=109^\circ$ <sup>(22)</sup> at room temperature. The detailed structural analyses on the crystal and the temperature variation has not been reported by the X-ray or neutron diffraction methods.

There, however, have been the X-ray studies on other rare earth compound crystals, such as La, Ce, Pr, Nd, Gd and Y<sup>(23)</sup>. The X-ray diffractometric studies have confirmed the crystal triclinic and shown that there exists two isostructural series, both crystallizing in the space group  $\text{P}\bar{1}$ ; La and Ce belongs to the first series, and Pr . . . Lu and Y to the second.

The structure of  $\text{La}(\text{NO}_3)_3 \cdot 6\text{H}_2\text{O}$ <sup>(24)</sup> has been revealed by X-ray study that  $\text{La}^{+3}$  is surrounded by 11 oxygens, from three  $\text{NO}_3^-$  groups and from five  $\text{H}_2\text{O}$  molecules. The other rare earth series (Nd, Pr)<sup>(25)</sup>, the coordination number is 10. The trivalent rare earth compound  $[\text{R}(\text{H}_2\text{O})_n(\text{NO}_3)_3]$  ( $n=1$  or  $2$ ) and the rest outer-sphere water molecules are joined into a three-dimensional structure by hydrogen bonds. The network of hydrogen bonds has been found in a ferroelectric crystal, such as Rochelle salt and  $\text{KH}_2\text{PO}_4$ , and plays an important role of the phase transition<sup>(26)</sup>.

The results in this study may suggest the possibility of the two three phases I, II and III, given in Figs. 15 and 16, for the samarium nitrate crystal. The phase transitions may be related to the variation in the complex structure, by the hydrogen bonds, attributed to the characteristic electronic property of the rare earth ion,  $\text{Sm}^{+3}$ , in the crystal.

## 5. Summary

- 1) From the observation of the temperature dependence of ultraviolet absorption spectrum in the

Report on the optical and electric properties  
of the nitrate compound crystals

alkali nitrate crystal, the variation in the coupling between the electronic process and lattice system could be found at the various phase transition points.

- 2) From the measurements of the frequency and temperature dependence of AC conductivity in the alkali nitrate crystal, we have obtained experimental information on the changes of ionic conduction in the various phases accompanied with the changes of the crystal structure at the first order phase transition points.
- 3) From the measurements of temperature dependence of dielectric constant in the rare earth nitrate crystals, polymorphic transitions have been found.

### References

- (1) C. N. R. Rao and K. J. Rao: Phase transitions in Solids, An Approach to the Study of the Chemistry and Physics of Solids (McGraw-Hill Inc., New York, 1978), H. E. Introduction to phase transitions and critical phenomena, (Clarendon Press, Oxford, 1971).
- (2) R. Kawashima and K. Suzuki: J. Phys. Soc. Jpn 52 (1983) 1857., R. Kawashima, K. Katsuki and K. Suzuki: Phys. Stat. Sol. (b) 129 (1985) 697, R. Kawashima, et. al.: Phys. Lett. 111A (1985) 304, R. Kawashima: Sol. Stat. Commun. 57 (1986) 265, R. Kawashima, K. Katsuki and K. Suzuki: J. Phys. Soc. Jpn. 54 (1985) 2057, R. Kawashima; J. Phys. C. Solid State Phys. 19 (1986) L759.
- (3) R. Kawashima, K. Katsuki and K. Suzuki: J. Phys. Soc. Jpn. 54 (1985) 2057, R. Kawashima and T. Uchiumi: Solid State Commun. 58 (1986) 625, R. Kawashima and T. Uchiumi: J. Phys. Soc. Jpn. 550 (1986) 3143, R. Kawashima and K. Hirai to be published in Philo. Mag. R. Kawashima and T. Matuda to be published in Phys. Stat. Sol. (a) 108.
- (4) R. N. Brown and A.C. McLaren: Acta Cryst. 15 (1962) 974.
- (5) K. L. McEwen: J. Chem. Phys. 34(1961)547.
- (6) G. P. Smith and C. R. Boston: J. Chem. Phys. 34 (1961) 1396.
- (7) H. Sumi and Y. Toyozawa: J. Phys. Soc. Jpn. 31 (1971) 341, M. Schreiber and Y. Toyozawa: J. Phys. Soc. Jpn. 51 (1982) 1528, 1537, 1544, 53 (1984) 864.
- (8) V. I. Zametin, M. A. Yakubovskii and L. M. Rabkin: Sov. Phys. Solid State 21 (1979) 291, V. I. Zametin: Phys. Stat. Sol. (b) 124 (1984) 625.
- (9) Y. Toyozawa: Prog. Theor. Phys. 20 (1958) 64.
- (10) T. Kakitani: J. Phys. Soc. Jpn. 55 (1986) 993.
- (11) T. Mitsui, ed.: Landolt-Bornstein, Vol. 16, Ferroelectrics and Related substances (Springer-Verlag, Berlin, Heidelberg, New York, 1982).
- (12) W. Rehwald: Adv. Phys. 22 (1973) 721.
- (13) J. Hladik ed.: Physics Electrolytes Vol. 1 (Academic Press London, New York, 1972).
- (14) P. P. Salhotra, E. C. Subbaro and P. Venkateswarlu: Phys. Status Solidi 29 (1968) 859 and 31 (1969) 233, S. W. Kennedy: Phys. Status Solidi (a) 2 (1970) 415.
- (15) F. A. Grant: J. Appl. Phys. 29 (1985) 76.
- (16) Vera V. Daniel: Dielectric Relaxation (Academic Press London New York, 1967).
- (17) A. Chen and F. Chernow: Phys. Rev. 154 (1967) 498.
- (18) M. Shamsuzzoha and B. W. Lucas: Acta Cryst. B38 (1982) 2353.
- (19) B. Jezowska-Trzebiatowska, J. Legendriewicz and W. Strek ed., Rare Earths Spectroscopy, Proceedings

- of the International Symposium on Rare Earths Spectroscopy (World Scientific Publishing Co. Pte. Ltd., 1985).
- (20) P. Wachter and H. Boppard ed., Valence Instabilities, Proceedings of the International Conference on Valence Instabilities (North-Holland Publishing Co., Amsterdam, New York, Oxford, 1982).
  - (21) J. G. Bednorz and K. A. Mulller, Z. Phys. B. Cond. Matt. 64, 159–193 (1986).
  - (22) M. Quarton and D. Svoronos, J. Solid State Chem. 42 (1982) 324.
  - (23) K. A. Gshneider Jr. and L. Eyring, ed., Handbook on the Physics and Chemistry of Rare Earths Vol. 8 p302–334 (North-Holland Publ. Co., Amsterdam, 1986).
  - (24) B. Eriksson et. al., Inorg. Chem. 19 (1980) 473.
  - (25) G. F. Volodina, I. M. Rumanova and N. V. Berov, Sov. Phys. Cryst. 6 (1962) 741.
  - (26) P. Schuster et al. ed., The hydrogen bond—recent developments (North-Holland Publ. Co., Amsterdam, 1976). Chapter 23 Ferroelectric hydrogen bonded systems, by V. H. Schmidt.